ACS APPLIED ENERGY MATERIALS

www.acsaem.org
Article

The Effect of Electronic Band Structure on High-Temperature Photovoltage Generation in CeO_2-Based Oxides

Yuki Morita,* Mina Yamaguchi, Riyan A. Budiman, Keiji Yashiro, and Tatsuya Kawada

Cite This: ACS Appl. Energy Mater. 2026, 9, 1499−1507
Read Online

ACCESS | Metrics & More | Article Recommendations | Supporting Information

ABSTRACT: High-temperature photovoltage generation, driven by UV-enhanced oxygen incorporation, was investigated by using ionic conductive oxides with a fluorite-type structure. To elucidate the role of photoexcited electrons in this process, the UV photoresponse of CeO_2 doped with various rare earth elements (Gd, La, Sm, Y, and Pr) and Y-doped ZrO_2 was compared. Samples were irradiated with UV light at a central wavelength of 365 nm, and the open circuit voltage between the illuminated and nonilluminated surfaces was measured. A clear voltage increase, suggesting enhanced oxygen uptake, was observed in Gd-, La-, Sm-, and Y-doped CeO_2, whereas Pr-doped CeO_2 and Y-doped ZrO_2 exhibited no increase. In Pr-doped CeO_2, the Pr 4f band, located within the band gap, traps photoexcited electrons and accelerates electron−hole recombination. This mechanism prevents electrons and holes from participating in the reactions. In Y-doped ZrO_2, the band gap is too large for UV excitation. These findings indicate that both the absence of impurity bands and the presence of UV absorption are essential for high-temperature photovoltage generation. This provides guidelines for discovering new materials and designing devices for solar-to-chemical energy conversion.

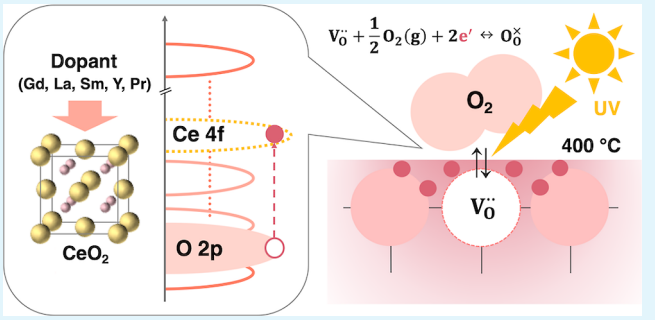

KEYWORDS: *high-temperature, CeO_2, ionic conductor, mixed conductor, band structure, photoexcitation, photovoltage, surface exchange reaction*

INTRODUCTION

Since their discovery in the 1800s, solid-state ionic materials have been studied extensively.[1,2] Among these materials, oxide ion conductors have found applications in various devices, such as solid oxide fuel cells (SOFCs), solid oxide electrolysis cells (SOECs), oxygen separation membranes, syngas conversion membranes, and gas sensors.[3,4] Some solid-state ionic oxides have been found to exhibit photoresponses, such as photo-induced defect formation,[5,6] photoenhanced ionic conductivity,[7] or photovoltage generation,[8] even at elevated temperatures. Among oxide ion conductors, $SrTiO_3$ (STO)- and CeO_2-based materials have been reported to generate photovoltage when irradiated with UV light.[9−14] This mechanism is attributed, in part, to photoinduced oxygen uptake from the surrounding gas phase, which creates an oxygen chemical potential gradient within the oxide.[9−12,15] In particular, certain STO-based cells have been shown to generate voltages exceeding 1 V depending on the specific material combination used.[12] These materials are considered promising for application in solid oxide photoelectrochemical cells (SOPECs), which have the potential to convert light energy into electrical and even chemical energy.[10−13,15−17]

Previous studies on the photoresponse of STO focused on UV effects on its properties at high temperatures (540−730 °C). These studies suggested that UV irradiation enhances the oxygen uptake reaction in Fe-doped STO.[17,18] Meanwhile, high-temperature photovoltage generation was observed in n-type Nb-doped STO at a Schottky junction but was to be unrelated to ionic properties.[19−21] A later report in 2016 on p-type STO with certain oxide ion conductivity at elevated temperatures (around 300 °C)[11] marked the first observation of photovoltage generation due to oxygen uptake, i.e., the conversion of light energy to chemical energy under UV irradiation at elevated temperatures. Impedance spectroscopies and oxygen permeability tests have provided strong experimental evidence that UV irradiation enhances oxygen uptake.[10−14] Additionally, isotopic exchange and secondary ion mass spectrometry analysis have indicated that UV irradiation enhances the surface exchange reaction and reduces the ionic space-charge potential.[22] Although a report has indicated that no enhancement of the surface exchange reaction is observed in highly Fe-doped STO,[23] several previous studies have reported that electron−hole pairs

Received: October 13, 2025
Revised: January 19, 2026
Accepted: January 19, 2026
Published: January 22, 2026

generated by UV irradiation,[10,15] particularly the substantial increase in conduction band electrons,[14,17,18] promote the oxygen uptake reaction.

More recently, high-temperature photovoltage generation has also been observed with CeO_2-based oxides, which function as nearly pure oxide-ion conductors in an oxidizing atmosphere. Indeed, CeO_2 has been extensively studied for its ionic conductivity and photocatalytic activity at room temperature.[3,24,25] These two properties have been considered separately, and the combined effect is yet to be discussed. Shi et al. reported photovoltage generation in an electrochemical cell employing undoped and Sm-doped CeO_2 films deposited on yttria-stabilized zirconia (YSZ).[9] In addition, previous research demonstrated that Gd-doped CeO_2, even in its sintered ceramic form, exhibits photovoltage at 300−450 °C and the photovoltage strongly depends on a wavelength and an intensity of a light source.[26] These reports revealed that UV-induced enhancement of oxygen uptake occurs in doped CeO_2 similarly to that in STO-based oxides and that electrons photoexcited to the Ce 4f band are involved in this reaction. However, to the best of our knowledge, the detailed mechanism and specific conditions under which photoexcited electrons in doped CeO_2 enhance oxygen incorporation remain to be fully elucidated. These insights are necessary to discover materials that generate photovoltage and to design cells that convert solar energy into chemical energy.

Given that photoexcited electrons in the Ce 4f band promote the oxygen uptake, when these electrons are unavailable—for example, being trapped in impurity bands—photovoltage generation is suppressed. Since CeO_2 can be doped with various rare earth elements having different d- or f-band energies, it is expected that the band structure can be controlled or that an impurity band can be formed in the band gap by changing the dopant species. Thus, this study compares the high-temperature photoresponses of CeO_2 doped with different elements to elucidate the mechanism and conditions by which photoexcited electrons contribute to high-temperature photovoltage generation in CeO_2-based oxides. For comparison, YSZ, a well-established ionic conductor,[3,27] was investigated.

EXPERIMENTAL SECTION

The following materials were used: CeO_2 doped with 10% Gd, La, Sm, Y, and Pr (denoted as GDC, LDC, SDC, YDC, and PDC, respectively), as well as YSZ (8% Y_2O_3−ZrO_2). The GDC, LDC (both from Shin-Etsu Chemical Co., Ltd.), and YSZ (Tosoh Co., Ltd.) powders were purchased commercially. The SDC and YDC powders were synthesized by coprecipitation, and the PDC powder was synthesized by the Pechini method. The coprecipitation involved dissolving Sm_2O_3, Y_2O_3 (Kojundo Chemical Lab. Co., Ltd.), and CeO_2 (Rare Metallic Co., Ltd.) in nitric acid (Wako Pure Chemical Corp.) in a stoichiometric ratio. The oxalates were then precipitated by adding oxalic acid (Wako Pure Chemical Corp.) and calcined at 900 °C to obtain the desired powder. In the Pechini method, $Pr(NO_3)_3$ and $Ce(NO_3)_3$ were mixed, and citric acid (Wako Pure Chemical Corp.) and ethylene glycol (Kanto Chemical Co., Inc.) were added, and the mixture was stirred thoroughly. The solution was gradually heated to 400 °C to form a gel. The resulting gel was subsequently calcined at 900 °C to obtain the final powder.

All of the powders were compacted using uniaxial and isostatic pressing and then sintered at 1550 °C for 6 h with an electric furnace (Koyo Thermo Systems Co., Ltd.). The pellets were polished on both sides, ultrasonically cleaned, dried thoroughly, and ozone-ashed. The final pellets had an approximate diameter of 9 mm and a thickness of 1 mm. Table S1 summarizes the relative density of each pellet, all of which are above 95%. Platinum electrodes were deposited to a thickness of approximately 300 nm by using magnetron sputtering and an ion coater (Shinkuu Device Co., Ltd., Japan). The working electrode (WE) was designed with a comb-shaped structure to allow UV light to reach the oxide surface, while the counter electrode (CE) was circular with a diameter of 6 mm (Figure 1).

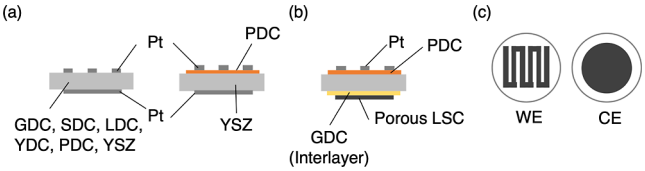

Figure 1. Cells prepared for (a) open circuit voltage (OCV) measurement, (b) electrochemical impedance spectroscopy (EIS) measurement, and (c) the shape of the electrodes.

Thin films of PDC were prepared by using pulsed laser deposition (PLD). A 10 Hz quadruple pulse from a YAG laser (Precision II, Continuum, San Jose, CA, USA) was used to deposit PDC onto polycrystalline YSZ pellets. PDC thin film was also deposited onto quartz substrates for optical property evaluation. Deposition was carried out at a substrate temperature of 750 °C under an oxygen pressure of 1.0 Pa. Following deposition, the sample was exposed to O_2 at a pressure of 100 kPa and annealed for 1 h to ensure proper film quality. The resulting film had a thickness of approximately 400 nm. For EIS measurements, a cell was made with a PDC thin film on a YSZ substrate, with a porous $La_{0.6}Sr_{0.4}CoO_{3-\delta}$ (LSC) CE. To ensure stability and prevent a reaction between the YSZ and the LSC, a 250 nm-thick GDC film was deposited on the CE side using PLD. Then, LSC paste was applied to the film and sintered at 1050 °C. Schematics of the cells are shown in Figure 1, and a summary of the prepared samples is provided in Table 1.

Table 1. Materials and Usage of Samples

measurement	oxides		WE	CE
OCV	bulk	GDC	comb shapes Pt sputtering	φ6 mm Pt sputtering
		SDC		
		LDC		
		YDC		
		PDC		
		YSZ		
	thin film	PDC (YSZ substrate)		
EIS	thin film	PDC (YSZ substrate)		porous LSC (GDC interlayer)

X-ray diffraction (XRD) measurements were performed on the finished pellets using a D2 PHASER (Bruker AXS GmbH, Germany) with Cu Kα radiation (λ = 1.5418 Å) to characterize the present phases.

Diffuse reflectance spectroscopy (DRS) was employed to assess the optical properties of the materials by using powders. The measurements were performed with a U-4000 spectrophotometer (Hitachi High-Tech Corp., Japan) operated with UV solutions software (Hitachi High-Tech Corp., Japan). MgO powder was utilized as both a reference and a diluting agent. Relative reflectance (%R) against MgO was measured across the 240−1000 nm wavelength range. The Kubelka−Munk (K−M) transformation was applied to calculate the absorption.

Spectroscopic ellipsometry (SE) was conducted (M-2000, J.A. Woollam Co., Inc., USA) to evaluate the absorption properties of the PDC thin film. Measurements were taken over a wavelength range of 200−1000 nm. The data were analyzed using complete ease software (J.A. Woollam Co., Inc., USA), and peak fitting was carried out using

https://doi.org/10.1021/acsaem.5c03218
ACS Appl. Energy Mater. 2026, 9, 1499−1507

Tauc-Lorentz oscillators.[28] A multilayer model that included back-surface reflection was applied to calculate the optical constants of the thin film.

Photoluminescence (PL) measurements were also conducted to compare the emission intensity of doped CeO_2 using a spectrofluorometer (F-2700, Hitachi High-Tech Analytical Science Corp., Japan). The measurements were performed on powdered samples at room temperature in air. CeO_2 powder was also measured for comparison. The spectral range was set from 300 to 700 nm, with an excitation wavelength of 300 nm.

Figure 2 depicts a schematic of electrochemical experimental equipment. The cell was placed in a silica glass chamber and inserted into a small furnace with a 5 mm diameter opening for UV illumination. The furnace was heated to maintain the pellets at approximately 400 °C. Pt meshes were pressed onto both the top and bottom of the cells with a spring load to ensure electrical contact. Air was supplied to both the WE and CE sides at a flow rate of 40 cm^3/m. A CL-H1-365-9-1-B light-emitting diode (LED) lamp (Asahi Spectra Co., Ltd., Japan) was placed at the bottom of the furnace to irradiate the cell with UV light (wavelength: 365 nm) from the opening through the Pt mesh. The distance between the light and the sample was 4 cm, and the intensity on the sample surface was approximately 1.1 W/cm^2.[26] Electrochemical measurements were conducted using an electrochemical measurement system (SP-300, Biologic, France). OCV measurements used a scan rate of 0.1 s, and EIS was performed with an amplitude of 50 mV over a frequency range of 1 MHz to 10 mHz.

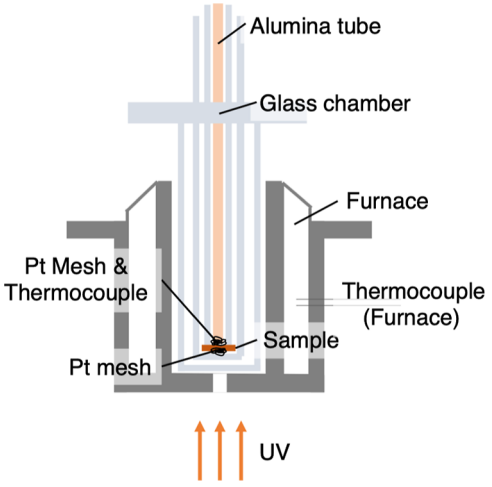

Figure 2. Setup of the electrochemical experiment.

RESULTS

Figure 3 presents the XRD patterns of the samples alongside reference patterns of fluorite-type CeO_2 and cubic ZrO_2 obtained from the Inorganic Crystal Structure Database (ICSD, FIZ Karlsruhe). No impurity peaks were observed in any of the samples. The PDC thin films on the YSZ pellets exhibited peaks corresponding to YSZ and PDC, indicating that the films grew properly.

Figure 4 shows the absorption intensity calculated from the DRS measurement. Since the original PDC powder exhibited strong absorption, leading to saturation of the absorption intensity, the only PDC was diluted with MgO powder at a weight ratio of 4:1 (MgO/PDC). Examining the doped CeO_2 samples, it can be seen that all of the doped CeO_2 materials have absorption edges in the energy region of the UV light used (λ = 365 nm). This absorption is attributed to the Ce 4f band, which is reported to be located approximately 3.3 eV

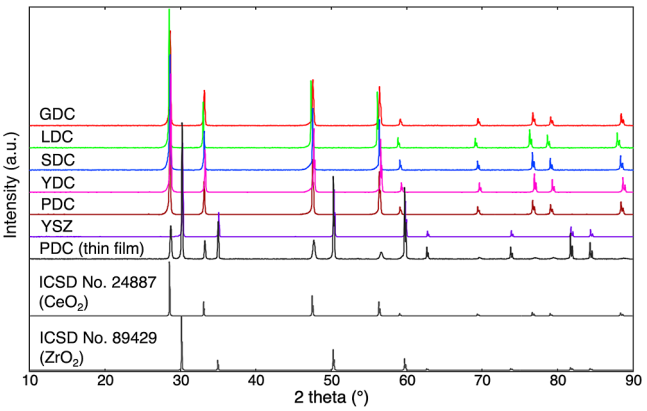

Figure 3. XRD patterns of the individual pellets and the thin film on the substrate, along with reference patterns from the ICSD (nos. 24887, 89429).

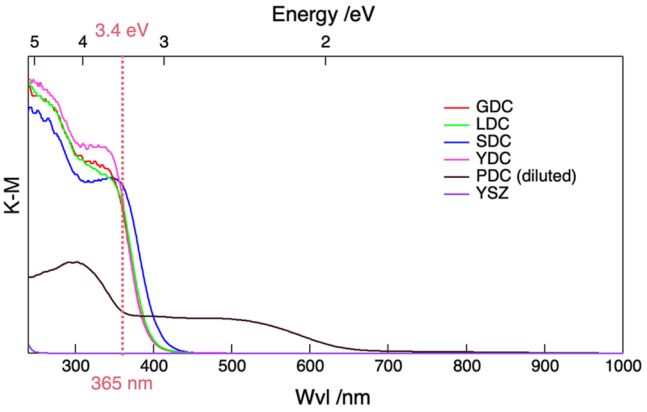

Figure 4. Absorption intensity of GDC, LDC, SDC, YDC, PDC, and YSZ powder, as calculated from DRS measurements. The dashed line represents the wavelength (365 nm) of the LED light source used for UV response in the electrochemical measurement.

higher than the O 2p band.[29−31] Additionally, the absorption edge of SDC shifted to the lower energy range, resulting from the Sm 4f band[9,32,33] (See the Discussion for details), and PDC exhibits a new absorption of longer wavelengths starting from around 650 nm, which is attributed to the Pr 4f band.[34−36] Similarly, light absorption in the lower energy region was also observed for the PDC thin film (Figure S1). In contrast, YSZ shows an absorption edge in a much higher energy region than doped CeO_2, near 250 nm. This is due to the Zr 4d band, which is approximately 5.6 eV higher than the valence band.[37,38] Compared to doped CeO_2, YSZ absorbs a minimal amount of UV light.

The resulting OCV measurements are shown in Figure 5. Like previous studies of STO and CeO_2 oxides,[9,10,15] the voltage without UV light is nonzero. This nonzero voltage is likely due to the relatively low measurement temperatures, under which factors such as temperature gradient could have influenced the results. Additionally, the magnitude of the photovoltage (the voltage difference between the UV-on and UV-off conditions) varied across the samples. However, these variations can be believed to arise from a difference in the individual samples rather than from material-dependent factors. Figure S2 shows the OCVs of other GDC samples prepared by the same process and measured under the same conditions. Including the result of GDC in Figure 5, the

https://doi.org/10.1021/acsaem.5c03218
ACS Appl. Energy Mater. 2026, 9, 1499−1507

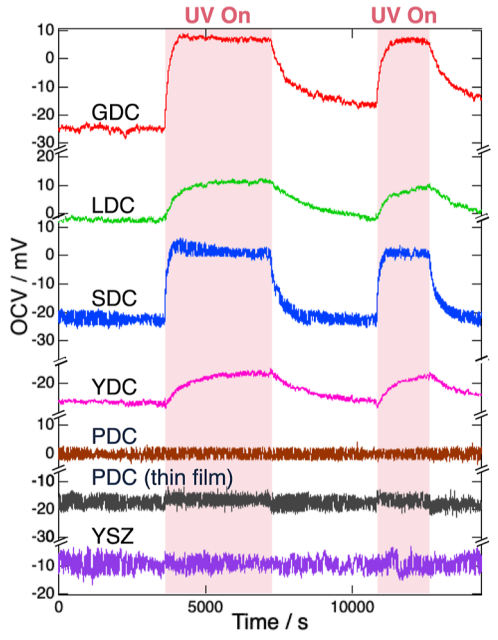

Figure 5. Photoresponse of doped CeO_2 and YSZ samples in an OCV setup with UV light activated and deactivated at 400 °C in air.

variation in the magnitude is evident among the samples. Similar variations have also been reported in previous studies of STO-based systems.[15] The exact cause remains unidentified, but several factors, including minor carrier conductivity and surface conditions, may be related to photovoltage generation and cause these variations. Despite the variations in the magnitude of the OCV among different GDC samples, measurement under repeated and long-term UV illumination confirmed that the magnitude of the OCV was consistently generated from materials exhibiting photoresponse, and no severe degradation leading to complete loss of voltage was observed (see Figures S3 and S4). Therefore, this study primarily focuses on the presence or absence of a response, while detailed comparison of magnitudes will be addressed in future work. The presence or absence of a response was determined based on whether the increase in photovoltage after irradiation exceeded 10 mV.

Regarding doped CeO_2, the results indicated a gradual increase in photovoltage during UV irradiation for GDC, SDC, LDC, and YDC. In contrast, PDC exhibited a negligible photoresponse. Given the high electronic conductivity of PDC in this atmosphere (see the Discussion), cells with PDC thin films deposited on YSZ substrates were prepared for electron blocking. However, the OCV remained unchanged under UV irradiation. Compared to the results of other bulk-doped CeO_2 and SDC thin films deposited on YSZ,[9] it is obvious that PDC did not exhibit any photoresponse. Additionally, the YSZ bulk exhibited no photoresponse to UV light. This result is reasonable in view of the SE measurements, which showed that YSZ does not absorb UV light. The band gap is approximately 5.6 eV, corresponding to the transition from the O 2p to Zr 4d orbitals.[37,38] This band gap is too high for electrons to be photoexcited by the UV light used in this experiment (365 nm: 3.4 eV), so no UV-enhancement occurred. The OCV measurements revealed high-temperature photovoltage generation in GDC, LDC, SDC, and YDC, whereas this was not observed in PDC and YSZ. The PDC sample showed no significant change in the OCV, even though it absorbed the wavelength of the light source as shown by the DRS and SE measurements, which indicates that electron photoexcitation from the O 2p band to the Ce 4f band is occurring.

Our previous studies have shown that a material generating photovoltage significantly decreases its electrode resistance under UV illumination.[26] To examine whether the electrode resistance in PDC changes, the EIS measurement was conducted. The results for the sample with the PDC thin film and YSZ substrate are shown in Figure 6a. The equivalent

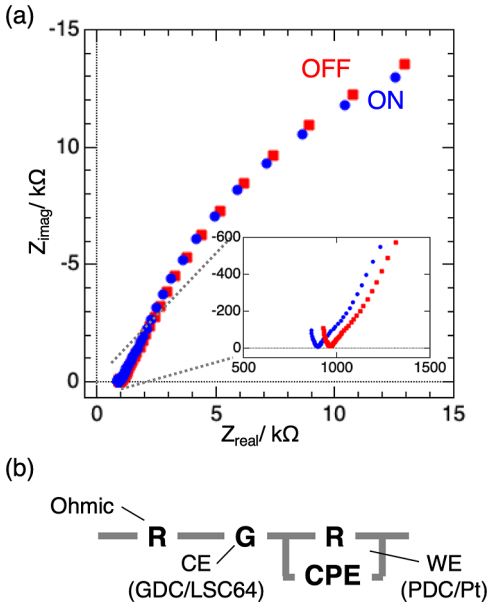

Figure 6. (a) The Nyquist plot of the EIS measurement results for the PDC thin film on the YSZ substrate. (b) The equivalent circuit model used for fitting.

circuit model employed to calculate the resistance values is shown in Figure 6b. It consists of a series connection of resistances (R), Gerischer elements (G), parallel circuits of resistances (R), and constant phase elements (CPE). These correspond to Ohmic resistance, CE resistance, and WE resistance, respectively. Figure S5 shows that the porous LSC electrode exhibits a much lower resistance than the Pt WE. Table 2 shows the obtained resistance values and the difference

Table 2. Resistance Values Obtained by Curve Fitting

	Ohmic/Ω	CE/Ω	WE/kΩ
UV off	978.10	442.23	43.412
UV on	910.04	409.83	44.125
Δ/%	6.9584	7.3265	5.2681

ratios between the UV-off and UV-on conditions. It can be seen that all of the resistances decrease slightly. These small changes are likely due to a temperature change of about 2 °C. This is in good agreement with the estimated temperature change of about 3 °C derived from the activation energy of a previous study[39] and the resistance values in this work (see detail in eq S1). Consequently, no significant change in the WE resistance by UV illumination was observed.

The results of the OCV and EIS measurements confirmed that PDC exhibited no photoresponse. As mentioned in the introduction, this suggests that changes in the band structure

https://doi.org/10.1021/acsaem.5c03218
ACS Appl. Energy Mater. 2026, 9, 1499−1507

caused by the addition of dopant to CeO_2 may contribute to the presence or absence of photovoltage generation. In this Discussion, possible factors that explain the lack of a photoresponse in PDC are considered.

DISCUSSION

General Properties of Doped CeO_2 and ZrO_2

Before the effect of UV radiation on doped CeO_2, the material properties are introduced. Then, the mechanism of the observed phenomena under UV irradiation is presented. CeO_2 and ZrO_2 are well-known for their ability to introduce oxygen vacancies and maintain electrical equilibrium when low-valence dopants are added. The equilibrium equation for the addition of trivalent dopants (M) is shown below

$$M_2O_3 \rightarrow 2M'_{Ce} + V_O^{\cdot\cdot} + 3O_O^{\times} \quad (1)$$

$$M_2O_3 \rightarrow 2M'_{Zr} + V_O^{\cdot\cdot} + 3O_O^{\times} \quad (2)$$

The introduced oxygen vacancies (V_O) are in equilibrium with gaseous oxygen at the material surface.

$$V_O^{\cdot\cdot} + \frac{1}{2}O_2 \rightarrow O_O^{\times} + 2h^{\cdot} \quad (3)$$

$$O_O^{\times} + 2h^{\cdot} \rightarrow V_O^{\cdot\cdot} + \frac{1}{2}O_2 \quad (4)$$

At high oxygen partial pressures, such as in the air used in this experiment, the reaction in eq 3 is more dominant than that in eq 4. Consequently, holes are abundant, and CeO_2 doped with fixed trivalent elements (Gd, La, Sm, and Y) and YSZ exhibit hole conductivity. On the other hand, Pr can undergo a redox transition between the 3+ and 4+ oxidation states, particularly at high oxygen partial pressures. Under these conditions, a large amount of Pr is oxidized.

$$Pr_{Ce}^{\cdot} \rightarrow Pr_{Ce}^{\times} + e' \quad (5)$$

This leads to an increase in the electronic conductivity in PDC.

The mechanism of the phenomenon under UV irradiation is as follows.[26] A schematic diagram is depicted in Figure 7. The

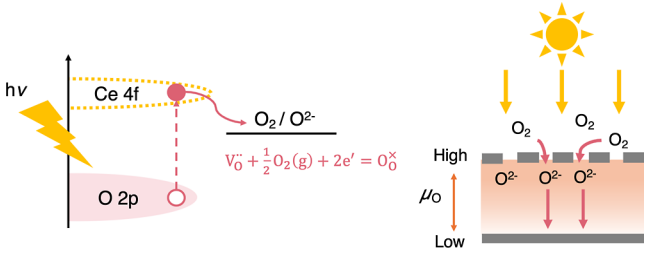

Figure 7. Oxygen equilibrium in doped CeO_2 under UV irradiation.

UV irradiation generates electron−hole pairs at the interface between Pt and CeO_2-based oxides. Specifically, electrons are excited from the O 2p band, which is at the top of the valence band, to the Ce 4f band at the bottom of the conduction band. This excitation increases the number of electrons in the conduction band. The energy of these electrons exceeds that required for oxygen incorporation. Thus, the increase in electrons promotes oxygen uptake by shifting the oxygen equilibrium between the gas and solid phases, the balance between eqs 3 and 4. Consequently, on the UV-irradiated side (the WE side), the oxygen potential (μ_O) increases. This is observed as a change in the electrochemical potential of electrons (or holes) in the mixed ionic-electronic conductor (MIEC), and it is detected as an increase in the OCV on the WE side.

Possible Reasons for the Absence of Photoresponse

After this overview, the discussion will address the three possible factors that explain the absence of a photoresponse in PDC.

(1) The ratio of electron and hole concentrations

In PDC, the valence of Pr changes between 3+ and 4+ depending on the oxygen partial pressure and temperature.[34−36,40,41] Specifically, under high oxygen partial pressures, the Pr 4f band exhibits n-type semiconductor-like behavior.[34] For instance, the carrier concentrations were calculated at 400 °C using the parameters measured by TG on the bulk PDC10 pellet between 600 and 900 °C in a previous report.[34] The details of the values used and the equilibrium equations can be found in Bishop et al.[34] As shown in Figure 8, at 400 °C in air, electrons (n) are more abundant than holes (h).

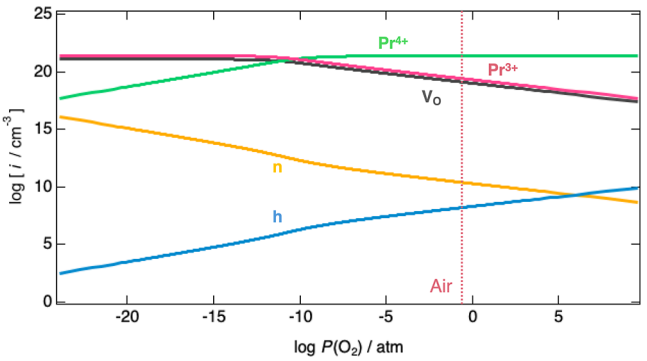

Figure 8. Carrier concentrations of PDC10 at 400 °C, as calculated using the parameters in ref 32.

Previous studies have shown that in p-type materials, the surface exchange reactions involve electrons as minor carriers in the rate-limiting reaction.[17,18,42,43] Then, the oxygen uptake is promoted because UV light generates electron−hole pairs, causing a significant increase in electrons compared to the amount present in the absence of UV irradiation.[14,17,18] In contrast, holes are minor carriers in PDC. Therefore, an increase in holes under UV irradiation could shift the equilibrium and enhance the oxygen emission. However, the OCV measurement results showed that PDC did not exhibit a photoresponse, indicating that neither oxygen uptake nor the emission occurred. Thus, it can be concluded that surface exchange reactions remain unaffected by the UV-generated carriers.

(2) Working electrode resistance on PDC

As mentioned in the Results, in a previous study, EIS measurements were conducted on GDC bulk pellets with a platinum WE at the same temperature. The results showed that UV irradiation largely reduces WE resistance, supporting the fact that UV irradiation enhances the oxygen uptake in GDC. However, Figure 7 shows that the WE resistance hardly changed by UV irradiation in PDC. A previous study has reported that PDC exhibits a faster surface exchange rate than

https://doi.org/10.1021/acsaem.5c03218
ACS Appl. Energy Mater. 2026, 9, 1499−1507

GDC, while also demonstrating that it can vary depending on experimental details.[44] In the present study, the WE resistance of PDC before UV irradiation was comparable to the reported values for GDC (tens of kΩ).[27] Therefore, the absence of a change of the WE resistance in PDC cannot be attributed to the initially low resistance. This result indicates that the surface reactions in PDC are unaffected by UV irradiation and suggests that the electrons and holes generated by UV irradiation are not utilized in surface exchange reactions in PDC.

(3) Electron trapping in the Pr 4f band

The valence of Pr in PDC changes between 3+ and 4+ depending on the oxygen partial pressure and temperature, leading to changes in the optical properties of the material.[34−36,40,45] In particular, the Pr 4f band in PDC is reported to be located about 2.1 eV higher than the valence band. Under high oxygen partial pressure, it appears between the O 2p and Ce 4f bands due to the Pr 4f band becoming empty.[34,35,45] As shown in Figure 7, $[Pr^{4+}]$ is much higher than $[Pr^{3+}]$, indicating that the Pr 4f band is almost completely unoccupied at 400 °C in air. Of the dopants introduced into CeO_2 in this study, only Pr exhibits a multiple oxidation state and introduces unoccupied impurity levels within the band gap; the others behave similarly to Gd (see eqs 1 and 5). The presence of these impurity levels originating from the Pr 4f band is considered to enable PDC to absorb relatively low-energy light. However, these impurity levels may also act as trap states, isolating photoexcited electron−hole pairs from the reaction.

Based on the above discussion of three possible factors, the third factor appears to be the most plausible. Based on these results, a mechanism for high-temperature photovoltage generation in doped ceria is proposed, along with an explanation for the absence of a photoresponse in PDC and YSZ (Figure 9).

Band Structure of Doped CeO_2 without UV Irradiation

Lanthanoids in their ionic state have well-shielded 4f orbitals, being located more inside than their 5s and 5p orbitals,[46] making 4f electrons predominately nonparticipating in chemical bonding. Although the 4f band hybridizes with the O 2p band to some extent in oxides,[47] it can be expected that the relative location of the 4f band is similar to that of isolated ions, even in the crystalline state. Thus, the magnitude of the ionization energy of the $4f^n/4f^{n+1}$ state of the atom[46,48,49] can reflect the relative energy height of the 4f band. In other words, as n, or the atomic number, increases, the energy level of the $4f^n/4f^{n+1}$ state, the 4f band, tends to decrease.

In doped CeO_2, the top of the valence band mainly consists of the O 2p band. Some theoretical studies[29,33] show that the O 2p band is unoccupied because they do not consider oxygen vacancies. However, oxygen vacancies are introduced to maintain electronic charge neutrality, as described in eqs 1 and 4. Therefore, a few holes remain due to the reaction in eq 3, but the O 2p band is almost fully occupied.

Theoretical studies report that the Sm 4f band in SDC is in the band gap and mixed with the O 2p band, forming an unoccupied hybrid valence band.[29,30] The distinctive high hole conductivity of SDC has not yet been confirmed by experiments; only a slight difference has been observed.[50] Furthermore, Sm exists as a trivalent ion in CeO_2. Considering these points, the Sm 4+/3+ reduction, corresponding to the Sm 4f band, is thought to be almost complete, as well.

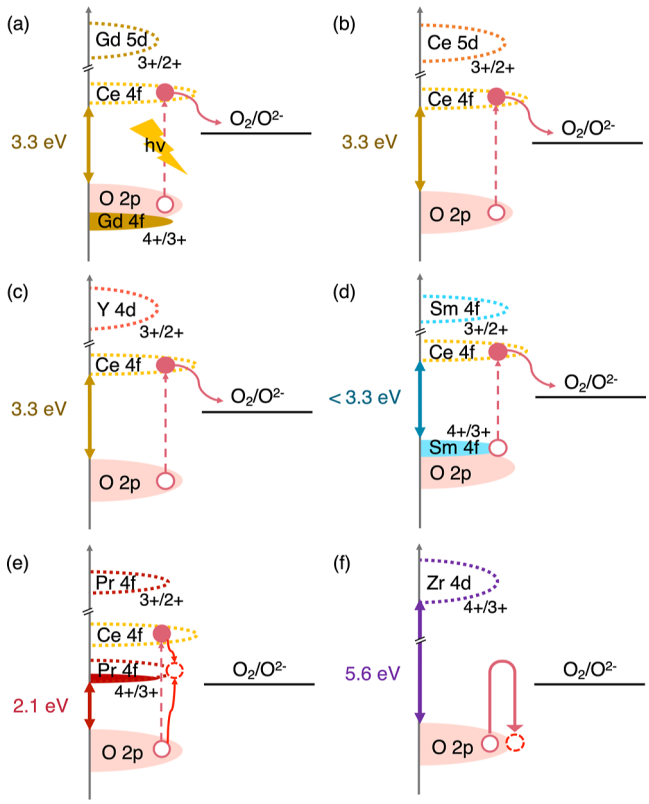

Figure 9. Band structures and the reaction energies for (a) GDC, (b) LDC, (c) YDC, (d) SDC, (e) PDC, and (f) YSZ.

In PDC, the Pr 4f band exists between the O 2p and the Ce 4f band. This band structure is similar to that of SDC, but the Pr 4f band is located at a much higher energy level than the Sm 4f band. Therefore, electrons prefer to exist in the O 2p band, which accompanies oxygen incorporation in oxidizing atmospheres, as shown in Figure 7. This makes the Pr 4f band unoccupied.

Phenomenon during UV Irradiation

In GDC, LDC, and YDC, UV light energy exceeds the band gap; therefore, electrons are photoexcited from the O 2p band to the Ce 4f band. The absence of an impurity band in the band gap[33,51] enables the photoexcited electrons to facilitate oxygen uptake.

In SDC, electrons are photoexcited not only from the O 2p band but also from the Sm 4f band, which is higher than the O 2p band. This band gap narrowing agrees with the shift of the absorption edge to lower-energy light in SDC (Figure 4) as well as slightly higher hole conductivity.[50] As with GDC, SDC has no impurity band; therefore, the photoexcited electrons are available for oxygen uptake.

In the case of PDC, an unoccupied Pr 4f band exists within the band gap. The ability of PDC to absorb lower-energy light (Figure 4) is likely due to a transition from the O 2p band to the Pr 4f band. This unoccupied Pr 4f band acts as an impurity band. Thus, the Pr 4f band traps electrons and holes and accelerates their recombination. The results of PL measurements for doped and undoped CeO_2 are presented in Figure S6. The large peaks around 300 and 600 nm in Figure S6a originate from scattering and residual excitation light, respectively, generated by the 300 nm irradiation source. Figure S6b shows an enlarged view of the emissions in the intermediate region. As CeO_2 powder is known as an indirect

https://doi.org/10.1021/acsaem.5c03218
ACS Appl. Energy Mater. 2026, 9, 1499−1507

bandgap material,[52,53] a band-edge emission was not observed clearly even in undoped CeO_2. On the other hand, most samples showed visible-range peaks, between 400 and 500 nm, which are attributed to defect states such as oxygen vacancies or dislocation.[54−58] In contrast, even defect-related emission was not observed in PDC, suggesting that the unoccupied Pr 4f band strongly acts as recombination centers. On typical photocatalysts, recombination of electron−hole pairs significantly affects the reactivity,[59−61] and an increased recombination rate caused by dopant-derived trap states deteriorates catalytic performance.[62,63] Therefore, in the surface oxygen exchange reaction at high temperatures, the enhanced recombination rate can also hinder the photoinduced reactions. Consequently, the accelerated recombination rate directs the photogenerated electrons and holes away from reactions, including oxygen uptake and emission.

Finally, YSZ has the Zr 4d band as the conduction band,[37,38] but as shown in Figure 4, this band is too high for electrons to be photoexcited by UV light with a wavelength of 365 nm. Consequently, photoexcitation in YSZ remains absent, and the electrons remain unavailable for reactions.

Previous studies have shown that oxygen uptake occurs in STO and TiO_2.[10,15] In this study, photovoltage was observed in doped CeO_2, except for PDC. These findings suggest that, for high-temperature photovoltage generation, not only is an oxygen vacancy important, but also the presence of bands capable of absorbing UV light, such as the Ce^{4+} 4f band (∼3.3 eV)[29−31] in CeO_2 and the Ti^{4+} 3d band (∼3.2 eV)[64−68] in TiO_2 and STO. Additionally, the absence of impurity bands that trap electrons is important. These insights are expected to contribute to the discovery of materials that exhibit high-temperature photovoltaic properties. They will also aid in the fabrication of cells that demonstrate desirable photoresponses, including high-temperature solar energy conversion systems for oxygen permeation and electrolysis.

CONCLUSIONS

This study compared the photoexcited electrons of various doped CeO_2 and YSZ under UV irradiation. Results from the DRS measurements showed that all doped CeO_2 absorbed UV light, whereas YSZ exhibited no UV absorption. Additionally, the absorption edge of SDC shifted toward lower energies, and PDC exhibited new absorption in the visible region. These features are attributed to the Sm 4f and the Pr 4f bands, respectively. From the OCV measurement, significant photoresponses were confirmed in GDC, LDC, SDC, and YDC, whereas no photoresponse was detected in PDC and YSZ. Although electrons are more abundant than holes in PDC, the EIS measurement shows that the oxygen uptake and emission were not to be facilitated. This indicates that the electrons and holes generated by UV irradiation are not utilized in the reactions. Based on these results, a mechanism for high-temperature photovoltage is proposed, and the absence of photovoltage in some materials is explained. In materials that exhibit photoreactions, the absence of an impurity band allows photoexcited electrons to participate in the reaction. Although the Sm 4f band in SDC lies in the band gap, it is almost fully occupied and thus does not act as the impurity band. In contrast, the unoccupied Pr 4f band exists in the band gap of PDC, trapping photoexcited electrons and holes and preventing their participation in the reactions. Conversely, YSZ has no impurity bands between the valence and conduction bands, but its bandgap is too large to allow photoexcitation of electrons. These results suggest that the absence of impurity bands and the presence of bands that absorb UV light are necessary for generating high-temperature photovoltage, providing guidelines for discovering materials that generate high-temperature photovoltage and for designing cells that exhibit desirable photoreactions.

ASSOCIATED CONTENT

Supporting Information

The Supporting Information is available free of charge at https://pubs.acs.org/doi/10.1021/acsaem.5c03218.

Pellet relative densities of each materials, absorption coefficient of PDC thin film on quartz, OCV measurement results from GDC samples, OCV measurement results of repeated UV illumination, OCV measurement results obtained under extended UV illumination, schematic of a symmetry cell with LSC electrodes and Nyquist plot, PL measurement results for CeO_2, GDC, LDC, SDC, YDC, and PDC powders, and calculation of average temperature within the sample after UV illumination (PDF)

AUTHOR INFORMATION

Corresponding Author

Yuki Morita − *Department of Advanced Social and Environmental Science, Graduate School of Environmental Studies, Tohoku University, Sendai 980-8579 Miyagi, Japan;* orcid.org/0009-0009-2027-8310; Email: morita.yuki.s2@dc.tohoku.ac.jp

Authors

Mina Yamaguchi − *Department of Advanced Social and Environmental Science, Graduate School of Environmental Studies, Tohoku University, Sendai 980-8579 Miyagi, Japan*

Riyan A. Budiman − *Department of Advanced Social and Environmental Science, Graduate School of Environmental Studies, Tohoku University, Sendai 980-8579 Miyagi, Japan; Research Center for Energy Materials, National Research and Innovation Agency (BRIN), South Tangerang 15314, Indonesia;* orcid.org/0000-0002-8566-8506

Keiji Yashiro − *Faculty of Materials for Energy, Shimane University, Matsue 690-8504 Shimane, Japan; Department of Advanced Social and Environmental Science, Graduate School of Environmental Studies, Tohoku University, Sendai 980-8579 Miyagi, Japan*

Tatsuya Kawada − *Department of Advanced Social and Environmental Science, Graduate School of Environmental Studies, Tohoku University, Sendai 980-8579 Miyagi, Japan*

Complete contact information is available at: https://pubs.acs.org/10.1021/acsaem.5c03218

Author Contributions

Y.M.: methodology, materials preparation, data curation, formal analysis, and writing—original draft. M.Y.: methodology and writing—review and editing. R.A.B.: methodology and materials preparation. K.Y.: methodology and supervision. T.K.: conceptualization, supervision, and writing—review and editing.

https://doi.org/10.1021/acsaem.5c03218
ACS Appl. Energy Mater. 2026, 9, 1499−1507

Funding

This work was partially supported in part by the Japan Society for the Promotion of Science (JSPS) under grants 23K19260 and 24K17515.

Notes

The authors declare no competing financial interest.

■ ACKNOWLEDGMENTS

Acknowledgments are extended to Prof. Hitoshi Takamura at Tohoku University for providing access to the spectroscopic ellipsometer and ozone asher system, and to Prof. Takahisa Omata at Tohoku University for allowing to use the diffuse reflectance spectrometer. Appreciation is also expressed to Assistant Prof. Tomoki Uchiyama (Tohoku University) and Assistant Prof. Takaya Fujisaki (Shimane University) for helpful discussions. Part of this study was conducted at the Micro/Nanomachining Research Education Center (MNC) at Tohoku University. Y. M. also acknowledges support from the GP-MS program at Tohoku University.

■ REFERENCES

(1) Funke, K. Solid State Ionics: From Michael Faraday to Green Energy—the European Dimension. *Sci. Technol. Adv. Mater.* **2013**, *14* (4), 043502.
(2) Knauth, P.; Tuller, H. L. Solid-State Ionics: Roots, Status, and Future Prospects. *J. Am. Ceram. Soc.* **2002**, *85* (7), 1654−1680.
(3) Skinner, S. J.; Kilner, J. A. Oxygen Ion Conductors. *Mater. Today* **2003**, *6* (3), 30−37.
(4) Steele, B. C. H. Oxygen Ion Conductors and Their Technological Applications. *Mater. Sci. Eng. B* **1992**, *13* (2), 79−87.
(5) Hensling, F. V. E.; Keeble, D. J.; Zhu, J.; Brose, S.; Xu, C.; Gunkel, F.; Danylyuk, S.; Nonnenmann, S. S.; Egger, W.; Dittmann, R. UV Radiation Enhanced Oxygen Vacancy Formation Caused by the PLD Plasma Plume. *Sci. Rep* **2018**, *8* (1), 8846.
(6) Siebenhofer, M.; Huber, T.; Artner, W.; Fleig, J.; Kubicek, M. Substrate Stoichiometry Changes during Pulsed Laser Deposition: A Case Study on $SrTiO_3$. *Acta Mater.* **2021**, *203*, 116461.
(7) Defferriere, T.; Klotz, D.; Gonzalez-Rosillo, J. C.; Rupp, J. L. M.; Tuller, H. L. Photo-Enhanced Ionic Conductivity across Grain Boundaries in Polycrystalline Ceramics. *Nat. Mater.* **2022**, *21* (4), 438−444.
(8) Siebenhofer, M.; Viernstein, A.; Morgenbesser, M.; Fleig, J.; Kubicek, M. Photoinduced Electronic and Ionic Effects in Strontium Titanate. *Mater. Adv.* **2021**, *2* (23), 7583−7619.
(9) Shi, Y.; Wang, L.; Wang, Z.; Vinai, G.; Braglia, L.; Torelli, P.; Aruta, C.; Traversa, E.; Liu, W.; Yang, N. Defect Engineering for Tuning the Photoresponse of Ceria-Based Solid Oxide Photoelectrochemical Cells. *ACS Appl. Mater. Interfaces* **2021**, *13* (1), 541−551.
(10) Fleig, J.; Walch, G.; Brunauer, C.; Rotter, B.; Esmaeli, E.; Summhammer, J.; Opitz, A. K.; Ponweiser, K. Mixed Conductors under Light: On the Way to Solid Oxide Photo-Electrochemical Cells. *ECS Trans.* **2016**, *72*, 23−33.
(11) Brunauer, G. C.; Rotter, B.; Walch, G.; Esmaeili, E.; Opitz, A. K.; Ponweiser, K.; Summhammer, J.; Fleig, J. UV-Light-Driven Oxygen Pumping in a High-Temperature Solid Oxide Photoelectrochemical Cell. *Adv. Funct. Mater.* **2016**, *26* (1), 120−128.
(12) Morgenbesser, M.; Schmid, A.; Viernstein, A.; de Dios Sirvent, J.; Chiabrera, F.; Bodenmüller, N.; Taibl, S.; Kubicek, M.; Baiutti, F.; Tarancon, A.; Fleig, J. $SrTiO_3$ Based High Temperature Solid Oxide Solar Cells: Photovoltages, Photocurrents and Mechanistic Insight. *Solid State Ionics* **2021**, *368*, 115700.
(13) Viernstein, A.; Kubicek, M.; Morgenbesser, M.; Walch, G.; Brunauer, G. C.; Fleig, J. High-Temperature Photochromism of Fe-Doped $SrTiO_3$ Caused by UV-Induced Bulk Stoichiometry Changes. *Adv. Funct. Mater.* **2019**, *29* (23), 1900196.
(14) Viernstein, A.; Kubicek, M.; Morgenbesser, M.; Huber, T. M.; Ellmeyer, E.; Siebenhofer, M.; Vaz, C. A. F.; Fleig, J. Mechanism of Photo-Ionic Stoichiometry Changes in $SrTiO_3$. *Solid State Ionics* **2022**, *383*, 115992.
(15) Walch, G.; Rotter, B.; Brunauer, G. C.; Esmaeili, E.; Opitz, A. K.; Kubicek, M.; Summhammer, J.; Ponweiser, K.; Fleig, J. A Solid Oxide Photoelectrochemical Cell with UV Light-Driven Oxygen Storage in Mixed Conducting Electrodes. *J. Mater. Chem. A* **2017**, *5* (4), 1637−1649.
(16) Schmid, A.; Baiutti, F.; Tarancon, A.; Fleig, J. A High Temperature Harvestorer Based on a Photovoltaic Cell and an Oxygen Ion Battery. *ACS Appl. Energy Mater.* **2024**, *7* (1), 205−213.
(17) Merkle, R.; De Souza, R. A.; Maier, J. Optically Tuning the Rate of Stoichiometry Changes: Surface-Controlled Oxygen Incorporation into Oxides under UV Irradiation. *Angew. Chem., Int. Ed.* **2001**, *40* (11), 2126−2129.
(18) Merkle, R.; Maier, J. Oxygen Incorporation into Fe-Doped $SrTiO_3$: Mechanistic Interpretation of the Surface Reaction. *Phys. Chem. Chem. Phys.* **2002**, *4* (17), 4140−4148.
(19) Horikiri, F.; Ichikawa, T.; Han, L. Q.; Kaimai, A.; Yashiro, K.; Matsumoto, H.; Kawada, T.; Mizusaki, J. Nb-Doped $SrTiO_3$-Based High-Temperature Schottky Solar Cells. *Jpn. J. Appl. Phys., Part 1* **2005**, *44* (11R), 8023.
(20) Kawada, T.; Ichikawa, T.; Han, L. Q.; Yashiro, K.; Matsumoto, H.; Mizusaki, J. High Temperature Schottky Barrier on N-Type $SrTiO_3$ and Its Sensitivity to Ambient Gases. *J. Electroceram.* **2004**, *13* (1), 715−719.
(21) Ni, H.; Da, S. L.; Zhao, K.; Kong, Y.-C.; Wong, H. K.; Zhao, S. Q. Temperature-Dependent Transport and Transient Photovoltaic Properties of $La_{2/3}Ca_{1/3}MnO_3$/Nb:$SrTiO_3$ Heteroepitaxial p-n Junction. *J. Appl. Phys.* **2012**, *112* (2), 023101.
(22) Schwenkel, D.; Kielgas, T.; Harrington, G.; De Souza, R. A. A Tracer Diffusion Study of Diverse Photo-Ionic Phenomena in Strontium Titanate. *Adv. Funct. Mater.* **2025**, No. e19571.
(23) Skiba, E. J.; Buckner, H. B.; Lee, C.; McKnight, G.; Wallick, R. F.; van der Veen, R.; Ertekin, E.; Perry, N. H. UV-Driven Oxygen Surface Exchange and Stoichiometry Changes in a Thin-Film, Nondilute Mixed Ionic Electronic Conductor, $Sr(Ti,Fe)O_{3-d}$. *J. Am. Chem. Soc.* **2024**, *146* (33), 23265−23277.
(24) Inaba, H.; Tagawa, H. Ceria-Based Solid Electrolytes. *Solid State Ionics* **1996**, *83* (1), 1−16.
(25) Montini, T.; Melchionna, M.; Monai, M.; Fornasiero, P. Fundamentals and Catalytic Applications of CeO_2-Based Materials. *Chem. Rev.* **2016**, *116* (10), 5987−6041.
(26) Yamaguchi, M.; Kurata, M.; Morita, Y.; Iwata, R.; Fuwa, S.; Ishii, A.; Takamura, H.; Yashiro, K.; Kawada, T. Origin of Ultraviolet-Induced High-Temperature Photovoltaic Response at Pt/Gd-Doped CeO_2 Interface. *Adv. Opt. Mater.* **2025**, *13* (33), No. e01971.
(27) Fergus, J. W. Electrolytes for Solid Oxide Fuel Cells. *J. Power Sources* **2006**, *162* (1), 30−40.
(28) Yamaguchi, M.; Ishii, A.; Oikawa, I.; Takamura, H. Black Titanium Oxynitride Thin Films Prepared by Nitrogen Plasma-Assisted Pulsed Laser Deposition for Flat-Panel Displays. *Appl. Surf. Sci.* **2020**, *534*, 147616.
(29) Skorodumova, N. V.; Ahuja, R.; Simak, S. I.; Abrikosov, I. A.; Johansson, B.; Lundqvist, B. I. Electronic, Bonding, and Optical Properties of CeO_2 and Ce_2O_3 from First Principles. *Phys. Rev. B* **2001**, *64* (11), 115108.
(30) Filtschew, A.; Hofmann, K.; Hess, C. Ceria and Its Defect Structure: New Insights from a Combined Spectroscopic Approach. *J. Phys. Chem. C* **2016**, *120* (12), 6694−6703.
(31) Goubin, F.; Rocquefelte, X.; Whangbo, M.-H.; Montardi, Y.; Brec, R.; Jobic, S. Experimental and Theoretical Characterization of the Optical Properties of CeO_2, $SrCeO_3$, and Sr_2CeO_4 Containing Ce^{4+} (f^0) Ions. *Chem. Mater.* **2004**, *16* (4), 662−669.
(32) Lim, D.-H.; Kim, H. S.; Yoon, S. P.; Han, J.; Yoon, C. W.; Choi, S. H.; Nam, S. W.; Ham, H. C. Mechanisms of Enhanced Sulfur Tolerance on Samarium (Sm)-Doped Cerium Oxide (CeO_2) from

https://doi.org/10.1021/acsaem.5c03218
ACS Appl. Energy Mater. 2026, 9, 1499−1507

First Principles. *Phys. Chem. Chem. Phys.* **2014**, *16* (22), 10727−10733.
(33) Xu, B.; Yang, H.; Zhang, Q.; Yuan, S.; Xie, A.; Zhang, M.; Ohno, T. Design and Synthesis of Sm, Y, La and Nd-Doped CeO_2 with a Broom-like Hierarchical Structure: A Photocatalyst with Enhanced Oxidation Performance. *ChemCatChem* **2020**, *12* (9), 2638−2646.
(34) Bishop, S. R.; Stefanik, T. S.; Tuller, H. L. Electrical Conductivity and Defect Equilibria of $Pr_{0.1}Ce_{0.9}O_{2-\delta}$. *Phys. Chem. Chem. Phys.* **2011**, *13* (21), 10165−10173.
(35) Kim, J. J.; Bishop, S. R.; Thompson, N.; Kuru, Y.; Tuller, H. L. Optically Derived Energy Band Gap States of Pr in Ceria. *Solid State Ionics* **2012**, *225*, 198−200.
(36) Bishop, S. R.; Chen, D.; Kuru, Y.; Kim, J.-J.; Stefanik, T.; Tuller, H. L. High Temperature Materials Division Outstanding Achievement Award Measurement and Modeling of Electrical, Mechanical, and Chemical Properties of a Model Mixed Ionic Electronic Conductor: Pr Doped Ceria. *ECS Trans.* **2011**, *33* (40), 51.
(37) Kosacki, I.; Petrovsky, V.; Anderson, H. U. Band Gap Energy in Nanocrystalline ZrO2:16%Y Thin Films. *Appl. Phys. Lett.* **1999**, *74* (3), 341−343.
(38) Heiroth, S.; Ghisleni, R.; Lippert, T.; Michler, J.; Wokaun, A. Optical and Mechanical Properties of Amorphous and Crystalline Yttria-Stabilized Zirconia Thin Films Prepared by Pulsed Laser Deposition. *Acta Mater.* **2011**, *59* (6), 2330−2340.
(39) Ahamer, C.; Opitz, A. K.; Rupp, G. M.; Fleig, J. Revisiting the Temperature Dependent Ionic Conductivity of Yttria Stabilized Zirconia (YSZ). *J. Electrochem. Soc.* **2017**, *164* (7), F790.
(40) Kim, J. J.; Bishop, S. R.; Chen, D.; Tuller, H. L. Defect Chemistry of Pr Doped Ceria Thin Films Investigated by in Situ Optical and Impedance Measurements. *Chem. Mater.* **2017**, *29* (5), 1999−2007.
(41) Chen, D.; Bishop, S. R.; Tuller, H. L. Non-Stoichiometry in Oxide Thin Films: A Chemical Capacitance Study of the Praseodymium-Cerium Oxide System. *Adv. Funct. Mater.* **2013**, *23* (17), 2168−2174.
(42) Jung, W.; Tuller, H. L. A New Model Describing Solid Oxide Fuel Cell Cathode Kinetics: Model Thin Film $SrTi_{1-x}Fe_xO_{3-\delta}$ Mixed Conducting Oxides−a Case Study. *Adv. Energy Mater.* **2011**, *1* (6), 1184−1191.
(43) Lane, J. A.; Kilner, J. A. Oxygen Surface Exchange on Gadolinia Doped Ceria. *Solid State Ionics* **2000**, *136*−*137*, 927−932.
(44) Schaube, M.; Merkle, R.; Maier, J. Oxygen Exchange Kinetics on Systematically Doped Ceria: A Pulsed Isotope Exchange Study. *J. Mater. Chem. A* **2019**, *7* (38), 21854−21866.
(45) Kim, J. J.; Bishop, S. R.; Thompson, N. J.; Chen, D.; Tuller, H. L. Investigation of Nonstoichiometry in Oxide Thin Films by Simultaneous in Situ Optical Absorption and Chemical Capacitance Measurements: Pr-Doped Ceria, a Case Study. *Chem. Mater.* **2014**, *26* (3), 1374−1379.
(46) Simon, C. *Lanthanide and Actinide Chemistry*; John Wiley & Sons, Ltd, 2006.
(47) Arai, F.; Kimura, S.; Ikezawa, M. Resonant Photoemission Study of Electronic Structure of Rare-Earth Sesquioxides. *J. Phys. Soc. Jpn.* **1998**, *67* (1), 225−229.
(48) Sugar, J.; Reader, J. Ionization Energies of Doubly and Triply Ionized Rare Earths. *J. Chem. Phys.* **1973**, *59* (4), 2083−2089.
(49) Sugar, J. Ionization Energies of Quadruply Ionized Rare Earths. *J. Opt. Soc. Am., JOSA* **1975**, *65* (11), 1366−1367.
(50) Xiong, Y.; Yamaji, K.; Horita, T.; Sakai, N.; Yokokawa, H. Hole and Electron Conductivities of 20 Mol % - $REO_{1.5}$ Doped CeO_2 (RE = Yb, Y, Gd, Sm, Nd, La). *J. Electrochem. Soc.* **2004**, *151* (3), A407.
(51) Aparicio-Anglès, X.; Roldan, A.; de Leeuw, N. H. Gadolinium-Vacancy Clusters in the (111) Surface of Gadolinium-Doped Ceria: A Density Functional Theory Study. *Chem. Mater.* **2015**, *27* (23), 7910−7917.
(52) Doping-Induced Modulation of Electronic Optical and Wetting Properties of CeO_2. *J. Phys. Chem. Solids* **2022**, *168*, 110820
(53) Azergue, F. Z.; Rami, R.; Assad, R.; Drissi, L. B. Effect of 3d Transition Metal Impurities Doping on Electronic and Magnetic Properties of CeO_2. *Solid State Commun.* **2023**, *371*, 115275.
(54) Toloman, D.; Popa, A.; Sonher, R. B.; Bortnic, R.; Marinca, T. F.; Perhaita, I.; Filip, M.; Mesaros, A.; Toloman, D.; Popa, A.; Sonher, R. B.; Bortnic, R.; Marinca, T. F.; Perhaita, I.; Filip, M.; Mesaros, A. Enhancing the Photocatalytic Activity and Luminescent Properties of Rare-Earth-Doped CeO_2 Nanoparticles. *Appl. Sci.* **2024**, *14* (2), 522.
(55) Khan, M. A. M.; Khan, W.; Ahamed, M.; Alhazaa, A. N. Microstructural Properties and Enhanced Photocatalytic Performance of Zn Doped CeO_2 Nanocrystals. *Sci. Rep* **2017**, *7* (1), 12560.
(56) Deus, R. C.; Cortés, J. A.; Ramirez, M. A.; Ponce, M. A.; Andres, J.; Rocha, L. S. R.; Longo, E.; Simões, A. Z. Photoluminescence Properties of Cerium Oxide Nanoparticles as a Function of Lanthanum Content. *Mater. Res. Bull.* **2015**, *70*, 416−423.
(57) Tamizhdurai, P.; Sakthinathan, S.; Chen, S.-M.; Shanthi, K.; Sivasanker, S.; Sangeetha, P. Environmentally Friendly Synthesis of CeO_2 Nanoparticles for the Catalytic Oxidation of Benzyl Alcohol to Benzaldehyde and Selective Detection of Nitrite. *Sci. Rep* **2017**, *7* (1), 46372.
(58) Leel, N. S.; Kiran, M.; Kumawat, M. K.; Alvi, P. A.; Vats, V. S.; Patidar, D.; Dalela, B.; Kumar, S.; Dalela, S. Oxygen Vacancy Driven Luminescence, Ferromagnetic and Electronic Structure Properties of Eu Doped CeO_2 Nanoparticles. *J. Lumin.* **2023**, *263*, 119981.
(59) Wu, Y.-H.; Yan, Y.-Q.; Deng, Y.-X.; Huang, W.-Y.; Yang, K.; Lu, K.-Q. Rational Construction of S-Scheme CdS Quantum Dots/In2O3 Hollow Nanotubes Heterojunction for Enhanced Photocatalytic H_2 Evolution. *Chin. J. Catal.* **2025**, *70*, 333−340.
(60) Cai, M.; Li, R.; Xie, Z.; Huang, J.; Zeng, Y.; Zhang, Q.; Liu, H.; Lv, W.; Liu, G. Synthesis of a Core-Shell Heterostructured MoS_2/$Cd_{0.9}Zn_{0.1}S$ Photocatalyst for the Degradation of Diclofenac under Visible Light. *Appl. Catal., B* **2019**, *259*, 118033.
(61) Zhang, D.; Zhang, D.; Wang, S.; Li, H.; Liu, J.; Pu, X.; Chen, P.; Qin, R.; Hu, H.; Cai, P. Synthesize Magnetic $ZnFe_2O_4$@C/$Cd_{0.9}Zn_{0.1}S$ Catalysts with S-Scheme Heterojunction to Achieve Extraordinary Hydrogen Production Efficiency. *J. Colloid Interface Sci.* **2024**, *657*, 672−683.
(62) Mahi, T. A.; Hossain, Q. S.; Nishat, S. S.; Ahmed, S.; Khan, M. N. I.; Bashar, M. S.; Jahan, S. A.; Akhtar, U. S.; Jahan, S.; Chowdhury, F.; Hossain, K. S.; Irfan, A.; Ahmed, I. Combined Experimental and First Principles Look into (Ce, Mo) Doped BiVO4. *Heliyon* **2024**, *10* (8), No. e29408.
(63) Wen, C.; Ni, X.; Han, M.; Yu, Y.; Liu, C.; Zhang, Y.; Zheng, B.; Feng, S. The Function of Photocatalytic Performance and Carrier Separation Efficiency Tuned by Doping Content in Homogeneous Photocatalysts. *Adv. Sci.* **2025**, *12* (25), 2501026.
(64) Hanaor, D. A. H.; Sorrell, C. C. Review of the Anatase to Rutile Phase Transformation. *J. Mater. Sci.* **2011**, *46* (4), 855−874.
(65) Beltrán, A.; Gracia, L.; Andrés, J. Density Functional Theory Study of the Brookite Surfaces and Phase Transitions between Natural Titania Polymorphs. *J. Phys. Chem. B* **2006**, *110* (46), 23417−23423.
(66) Baker, J. N.; Bowes, P. C.; Long, D. M.; Moballegh, A.; Harris, J. S.; Dickey, E. C.; Irving, D. L. Defect Mechanisms of Coloration in Fe-Doped SrTiO3 from First Principles. *Appl. Phys. Lett.* **2017**, *110* (12), 122903.
(67) Cardona, M. Optical Properties and Band Structure of $SrTiO_3$ and $BaTiO_3$. *Phys. Rev.* **1965**, *140* (2A), A651−A655.
(68) van Benthem, K.; Elsässer, C.; French, R. H. Bulk Electronic Structure of $SrTiO_3$: Experiment and Theory. *J. Appl. Phys.* **2001**, *90* (12), 6156−6164.

https://doi.org/10.1021/acsaem.5c03218
ACS Appl. Energy Mater. 2026, 9, 1499−1507